Solution Structures of Cyclosporin A and Its Complex with Dysprosium(III) in SDS Micelles: NMR and Molecular Dynamics Studies

Francesca Bernardi, Nicola D'Amelio, Elena Gaggelli,* Elena Molteni, and Gianni Valensin

Department of Chemistry and the NMR Center, University of Siena, Via A. Moro, 53100 Siena, Italy

Received: August 27, 2007; In Final Form: October 9, 2007

Cyclosporin A (CsA) is a cyclic naturally occurring peptide used to prevent graft rejection in organ transplantations. Its immunosuppressive activity is due to the formation of a complex with cyclophilin A (Cyp), in which the cis ^{9}MeLeu−^{10}MeLeu amide bond of CsA assumes a trans conformation. The mechanism of the conformational inversion has not been delineated, but it has been postulated that metal ions binding induces a conformational change that enables CsA to bind Cyp. In this work, we solved the structures of CsA in sodium dodecyl sulfate (SDS) micelles (which enhance its solubility and mimic the hydrophobic environment clinically used for drug delivery) and its complex with Dy(III) ion, whose coordination chemistry is frequently used to reproduce the effect of Ca(II). The paramagnetic properties of Dy(III) allowed us to build up a structure using proton relaxation enhancements, which remains stable in a MD simulation in the micelle environment.

Introduction

Cyclosporin A (CsA) is a cyclic naturally occurring peptide widely used in medicine to prevent graft rejection.[1] The immunosuppressive activity is due to the formation of a complex with its intracellular specific receptor cyclophilin A (Cyp), a peptidyl-prolyl cis−trans isomerase. Once formed, the binary complex is able to inhibit the enzymatic activity of calcineurin, a protein involved in the activation and proliferation of T-cells.[2−4]

CsA contains eleven aliphatic amino acids (Scheme 1) responsible for its highly hydrophobic character and its very low solubility in water (26.67 μg/mL at 25 °C).[5] The conformation of CsA is largely affected by the solvent. It was shown that in solvents of low polarity, such as $CHCl_3$, tetrahydrofuran (THF), or CH_3CN, a single conformation is largely predominant, where the hydrophobic side chains are exposed to the solvent, while amide protons are buried in the interior by the formation of intramolecular hydrogen bonds.[6−8] On the contrary, in solvents of high polarity, such as dimethylsulfoxide (DMSO) or CH_3OH, many conformations coexist with similar existential probabilities, making the structure determination by NMR difficult.[9,10]

The presence of *N*-methylated amide nitrogens, as a consequence of nonribosomal synthesis, favors, by itself, higher contents of cis peptide bond conformation;[11] accordingly, the structure of free CsA contains a cis peptide bond between residues 9 and 10.[6] Since this bond was found trans in the complex with Cyp solved by NMR and the peptidyl-prolyl isomerase activity of Cyp is not responsible for the conversion,[12−15] comprehension of the mechanism of interaction relies on understanding what drives such a cis−trans transition. From this point of view, it has been postulated that binding of metal ions induces the conformational change that enables CsA to bind Cyp. As a matter of fact, lithium ions were shown to induce the 9−10 cis−trans conversion of CsA in THF;[16] whereas cerium(III) and magnesium(II) ions were inducing the trans−cis isomerization of 5−6 and 3−4 peptide bonds, respectively, in acetonitrile.[17] Moreover, the excretion of essential elements, and calcium among them, is one of the side effects, together with nephrotoxicity, hypertension, and diseases of lipid metabolism, limiting clinical applications of CsA.[18,19] Studies on the CsA−calcium complex in acetonitrile have revealed a strong association constant, suggesting a possible ionophoric role of CsA.[20−22]

SCHEME 1: Chemical Structure of the CsA Molecule

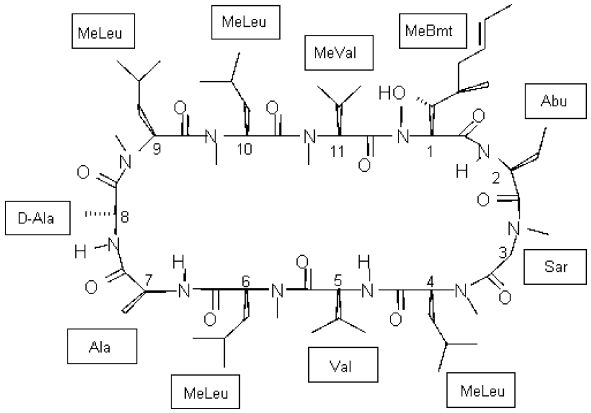

The NMR study on CsA in sodium dodecyl sulfate (SDS)−water micellar solution is herein reported. The choice of the system has been done for getting insight on the structure of CsA in more physiological conditions; the presence of SDS, in fact, enhances the solubility of CsA and mimics the hydrophobic environment provided by the drug delivery systems clinically used for drug administration.[23−25] The interaction between CsA and dysprosium(III), used as a paramagnetic probe for calcium(II), has also been investigated with the aim of further delineating the role of metal ions in the action mechanism of CsA. The use of lanthanides as a probe for calcium is due to their similar ionic radius and affinity toward oxygen atoms. Moreover, their paramagnetic properties make them well detectable where calcium is silent.

* Corresponding author. E-mail: gaggelli@unisi.it. Fax: (+39) 0577-234254.

10.1021/jp076837z CCC: $40.75
Published on Web 12/21/2007

Experimental Section

CsA was supplied by Sigma Chemical Co. (St. Louis, MO) and used without further purification. The sample was dissolved in water using SDS micelles to enhance CsA solubility. The concentrations of SDS and CsA were respectively 100 mM and 1.35 mM. The desired concentrations of Dy(III) were obtained using a stock solution of $DyCl_3$. Samples in pure water were instead 20 μM.

NMR experiments were acquired at 14.1 T on a Bruker Avance 600 MHz spectrometer at controlled temperatures ($\pm$0.2 K) using a TBI (triple broadband inverse) probe. TSP (trimethylsilyl-2,2,3,3-tetradeuteropropionic acid) was used as internal reference standard, with its resonance set to -0.017 ppm with respect to DSS (2,2-dimethyl-2-silapentane-5-sulfonic acid, 0.00 ppm).[26] Water suppression was achieved by excitation sculpting.[27] Proton resonance assignment was obtained through total correlation spectroscopy (TOCSY), correlation spectroscopy (COSY), and nuclear Overhauser effect spectroscopy (NOESY) standard experiments. The MLEV-17 pulse sequence, with a mixing time of 75 ms, was used for TOCSY. NOESY spectra were acquired at different values of mixing time in order to obtain the best one. Spin$-$lattice relaxation rates were measured with inversion$-$recovery pulse sequences or with a combination of this with two-dimensional (2D) TOCSY to gain resolution. This was obtained by introducing a ^{1}H 180° pulse followed by a variable delay in front of the TOCSY sequence. Relaxation rates (R_1) were calculated with regression analysis of the initial recovery curves of longitudinal magnetization components, leading to errors in the range $\pm$3%.

The solution structure of the free CsA in micelles was solved using NOE-based constraints. The intensities of NOESY cross-peaks of free CsA were converted into proton$-$proton distance constraints considering three motional classes and using as reference three cross-peaks related to proton pairs at fixed distance.[28]

The solution structure of the Dy(III) complex was based on metal$-$proton distance constraints calculated from R_1 values. Upper and lower distance limits were calculated using the minimum and maximum values of relaxation enhancements based on estimated R_1 error (3%). Metal$-$proton distance constraints obtained from relaxation enhancements smaller than the estimated error were used only as lower distance limits.

Constraints were exploited to build a pseudopotential energy for structural determination through a simulated annealing (SA) procedure in torsional angle space with the program DYANA.[29] The calculations were performed with 300 random starting structures of CsA and 10 000 steps of SA. Since only one molecule can be given as input in the program, for the complex, we linked the peptide to the metal ion through a long chain of linkers, that is, residues made by atoms without van der Waals radius. These linkers could freely rotate around their bonds, without causing steric repulsions, allowing us to sample a large number of relative positions of the ligand with respect to the dysprosium ion before the minimization step. Since CsA contains several nonstandard amino acids, the topologies of these residues were added to the DYANA library as described in.[17]

On the best structures obtained with this procedure, we performed an energy minimization followed by a molecular dynamics (MD) simulation, using the program GROMACS,[30,31] with the ffG43a2 force field.[32] In this case, the nonstandard amino acids were already present in the chosen force field, and the cyclization of the peptide was explicitly taken into account adding to its topology the necessary bonds, angles, and dihedrals, involving residues 11 and 1, defined as in a standard peptide bond between two consecutive residues. The simulations were performed placing the CsA molecule in the core of a pre-equilibrated SDS micelle, and the whole system was solvated using a parallelepiped box of water, with periodic boundary conditions, imposing a minimum distance between any atom of the peptide and the box edge of 1.5 nm and adding Na^+ ions in order to balance the negative charge of the micelle. After energy minimization, the system was brought to the temperature of 298 K through 6 molecular dynamics (MD) runs in each of which the temperature was raised by 50 K, followed by a MD run of 220 ps at constant temperature $T = 298$ K. The only constraints imposed on the CsA molecule were distance constraints of 0.20 to 0.26 nm between the dysprosium ion and its coordinating oxygens in the case of the complex. During the simulations, peptide, micelle, and solvent separately were weakly coupled to a temperature bath at the chosen temperature and to a pressure bath at 1 atm, with relaxation times $\tau_T = 0.1$ ps and $\tau_P = 0.5$ ps, respectively, using Berendsen's weak coupling algorithm;[33] bond lengths were constrained to equilibrium values using the SHAKE procedure,[34] with a geometric tolerance of 10^{-4}, and the time step was set to 2 fs. Nonbonded interactions were treated using a twin range method:[35] within a short-range cutoff of 0.8 nm, all interactions were determined at every time step, while longer range contributions within a cutoff of 1.4 nm were evaluated each time the pair list was generated.

In order to build the micelle, first we added the single SDS molecule topology to the chosen force field, then we arranged 60 SDS molecules in a roughly spherical shape; this initial micelle was subsequently equilibrated through an energy minimization and a molecular dynamics simulation in water with an appropriate number of Na^+ ions, imposing distance constraints equal to the largest dimension of the CsA structure between each of the terminal carbons of the hydrophobic tails and a dummy atom placed at the center of the micelle. During the equilibration, any water molecule inside the hydrophobic core of the micelle was removed.

Results

Structure of CsA in SDS$-$Water. The presence of SDS yields a ^{1}H NMR spectrum of CsA quite different from that in water at the same pH value of 6.5 (Figure 1), which demonstrates an interaction with the micelles. Inspection of the amide region shows that, while several conformations coexist in water with comparable intensities, one main species is singled out in SDS$-$water. A molecular interaction with SDS is also verified by the 3 orders of magnitude enhancement of CsA solubility. Since the chemical shifts of CsA are highly dependent upon SDS concentration, a titration was carried out until the spectrum remained unaffected. For a 1.35 mM sample, this was achieved at SDS concentration of 100 mM, far above the critical micelle formation limit (around 8 mM).[36]

The ^{1}H NMR assignment, reported in Table 1, was accomplished by homo-nuclear 2D experiments. The slower tumbling caused by the presence of micelles allowed us to obtain a wealth of structural information from the 2D NOESY experiment which led to a quite definite average structure of CsA in the SDS environment, shown in Figure 2A (for the best five structures backbone rmsd is 0.013 nm; 0.05 nm for the first 30). The structure reveals a cis conformation of the peptide bond between ^{9}MeLeu and ^{10}MeLeu, in agreement with what was observed in solvents of low polarity;[17] the cis conformation is demonstrated by a clear cross-peak between the Hα protons of 9 and 10 residues.

The involvement of mobile protons in hydrogen bonds was checked by measuring the temperature dependence of the chemical shift in the range 288$-$313 K. For residues 5 and 8, temperature coefficients less negative than -4.5 ppb/K (Figure 1 Supporting Information) suggest either the presence of a

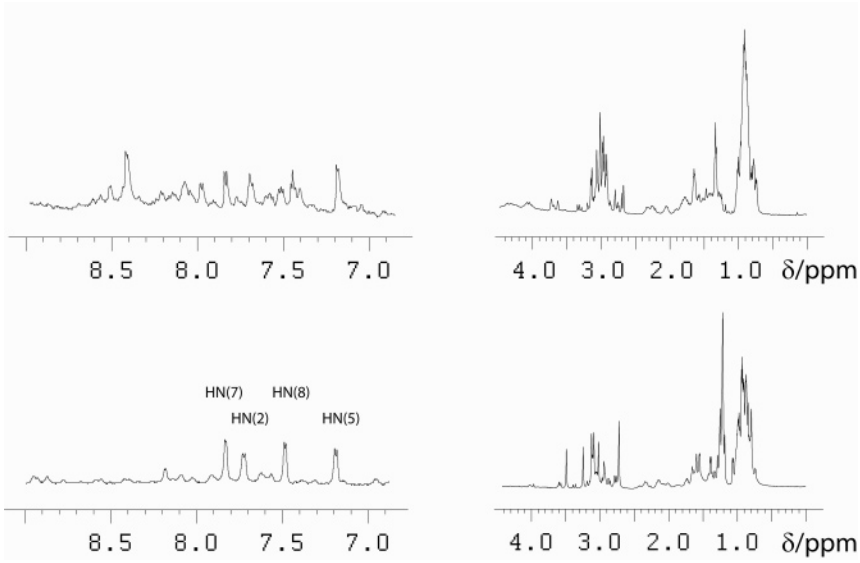

Figure 1. 1D spectra of free CsA in H_2O containing 100 mM of SDS micelles, pH = 6.5 (bottom) and free CsA in H_2O, pH = 6.5 (top).

TABLE 1: ^{1}H Chemical Shifts (Parts Per Million) of CsA 1.35 mM in SDS Micelles 100 mM at pH 6.5 and 298 K

	HN/HNMe	Hα	Hβ	Hγ	Others
^{1}MeBmt	3.50_5	5.24_5	4.03_5	1.60_5 γ	0.83_5 γMe, 2.36_5 δ, 2.02_5 δ′, 5.38_5 ζ
^{2}Abu	7.63_5	4.93_5	1.74_5 β, 1.62_5 β′	0.85_5	
^{3}Sar	3.25_5	4.88_5 α, 3.60_5 α′			
^{4}MeLeu	3.03_5	5.22_5	1.74_5 β, 1.49_5 β′	1.66_5	0.97_5 δ, 0.89_5 δ′
^{5}Val	7.12_5	4.72_5	2.15_5	0.97_5 γ, 0.90_5 γ′	
^{6}MeLeu	3.13_5	5.02_5	2.09_5 β, 1.32_5 β′	1.55_5	0.92_5 δ, δ′
^{7}Ala	7.76_5	4.31_5	1.40_5		
^{8}D−Ala	7.42_5	4.80_5	1.27_5		
^{9}MeLeu	3.09_5	5.64_5	2.15_5 β, 1.20_5 β′	1.41_5	0.99_5 δ, 0.89_5 δ′
^{10}MeLeu	2.73_5	5.20_5	2.36_5 β, 1.07_5 β′	1.69_5	1.08_5 δ, 1.02_5 δ′
^{11}MeVal	2.73_5	5.29_5	2.18_5	0.95_5 γ, 0.89_5 γ′	

hydrogen bond or poor solvent accessibility.[37] A more accurate analysis of the structure reveals that the presence of hydrogen bonds is spatially disfavored since the distance of each amide proton to the closest oxygen exceeds 0.3 nm. On the contrary, both amide protons of residues 5 and 8 display very low solvent accessibility (5% and 2.8%, respectively). All amide protons disappear upon dissolution of CsA in D_2O. Disappearance is however not sudden (few hours), revealing some kind of protection and supporting the assumption of the localization of the drug well inside the micelle.

It is known that the water concentration in micelles decreases from the surface toward the core of the micelle, with a completely hydrophobic (water-excluded) core. Therefore, the polarity of a solubilized molecule influences its spatial location in the micelle: nonpolar substances will be solubilized in the micellar core while those with intermediate polarity will be distributed along the surfactant molecules in intermediate positions.[25] The nonpolar character of CsA and the analysis of its potential surface in micelles, which indicates the exposition of hydrophobic regions (Figure 3A), also suggest the insertion of the molecule inside the micelle.

On the best experimental structure obtained with the simulated annealing procedure, an energy minimization and a molecular dynamics simulation in H_2O/SDS were performed with the CsA molecule placed in the core of the micelle (Figure 4A,B). The low value of backbone rmsd (0.05 nm), calculated on all the structures sampled along the MD trajectory and reported in Figure 4B, indicates a high conservation of the CsA structure. The electrostatic potential surface of the free CsA structure contains a negatively charged channel, which is conserved also in the average structure calculated on the MD trajectory after equilibration: ^{3}Sar and ^{11}MeVal are responsible for its negative charge.

Structure of the CsA−Dy(III) Complex. The addition of 0.3 equiv of Dy(III) to the CsA sample did not result in the appearance of a new set of signals, as reported for the CsA−Ca(II) complex in acetonitrile,[17] but determined a small change in chemical shift values in agreement with the formation of a complex in fast exchange with the free form, on the NMR time scale. In order to evaluate the effects of the metal ion, proton longitudinal relaxation rates (R_1) were measured and compared with those of the free form. The observed proton relaxation rate variations ΔR_1 (Figure 5) with a molar fraction of 1:0.3 clearly demonstrate a contribution from the interacting paramagnetic species. This is largely justified by the facts that (i) diamagnetic relaxation rates are dependent upon mobility which in turn is inversely proportional to the molecular weight (basically unaltered) and that (ii) paramagnetic effects are orders of magnitude more effective than small mobility changes.

Since protons are affected to a different extent, the measured effects refer to at least one well-defined conformation of the complex rather than to some long range nonspecific interaction. Because of the fast exchange between free and metal-bound CsA on the NMR time scale, the longitudinal relaxation rates measured upon metal addition equal the population-weighted average:

$$R_1^{obs} = p^{free}R_1^{free} + p^{bound}R_1^{bound}$$

$$R_1^{bound} = R_1^{para} + R_1^{dia} \cong R_1^{para} \quad (1)$$

where p^{free}, p^{bound} are the molar fractions, R_1^{free} is the longitudinal relaxation rate in the absence of the metal ion, R_1^{dia} and R_1^{para} are the diamagnetic and paramagnetic contribution to the relaxation rate in the presence of the paramagnetic species.

In order to obtain the paramagnetic contributions R_1^{para}, p^{free}, and p^{bound} must be evaluated. R_1^{para} depends on the correlation time modulating the dipolar interaction between the paramag-

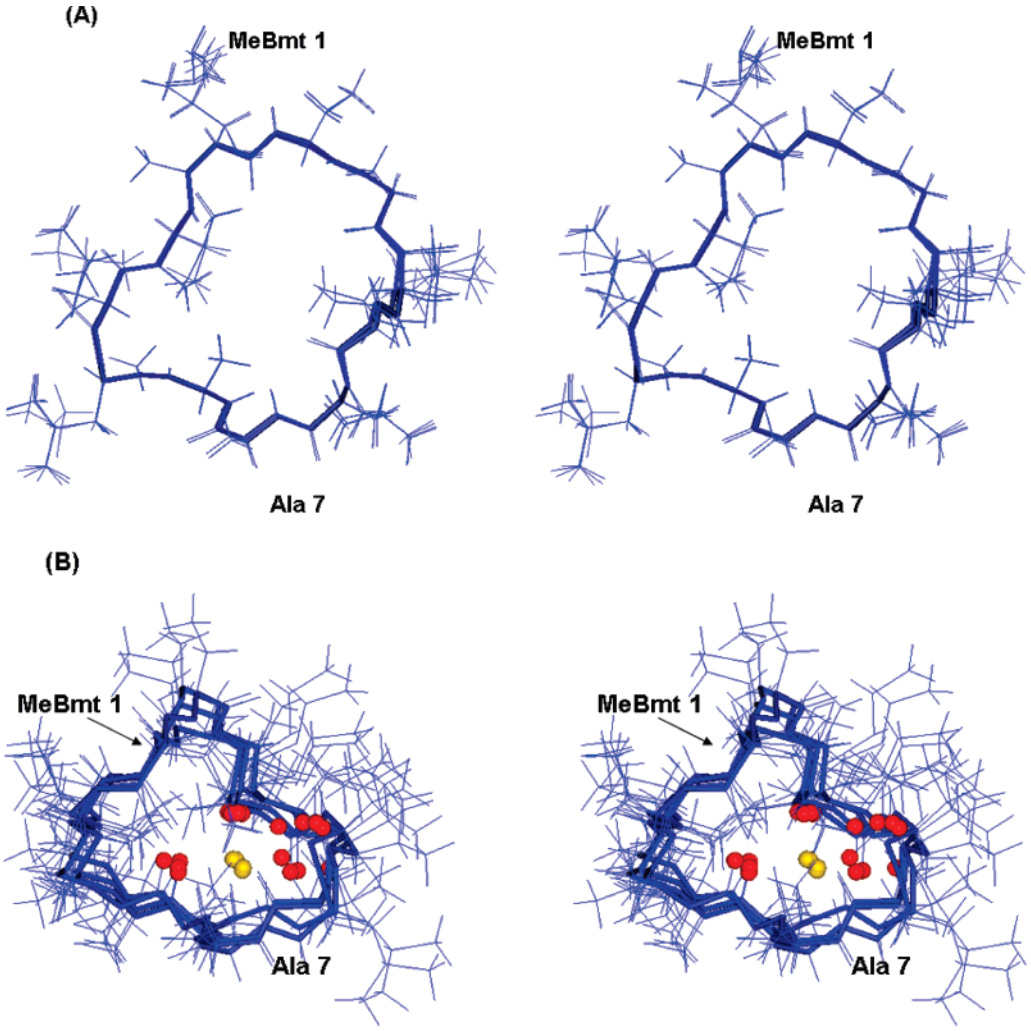

Figure 2. Best structures (stereo views) of (A) free CsA in micelles and (B) CsA-Dy(III) complex, with the metal ion shown in gold and the coordinating oxygens shown in red.

netic species and the nucleus and on their mutual distance, as described by the Solomon−Curie equation:[38]

$$R_1^{\text{para}} = R_{\text{Solomon}} + R_{\text{Curie}} + R_{\text{contact}} = \frac{2}{15}\left(\frac{\mu_0}{4\pi}\right)^2 \mu_B{}^2 g_J{}^2 \gamma_I{}^2 (J(J+1)) \frac{1}{r^6}\left\{\frac{\tau_{c2}}{(1+(\omega_I-\omega_S)^2\tau_{c2}{}^2)} + \frac{3\tau_{c1}}{1+\omega_I{}^2\tau_{c1}{}^2} + \frac{6\tau_{c2}}{(1+(\omega_I+\omega_S)^2\tau_{c2}{}^2)}\right\} + \frac{2}{5}\left(\frac{\mu_0}{4\pi}\right)^2 \frac{\mu_B{}^4 g_J{}^4 \omega_I{}^2 (J^2(J+1)^2)}{(3kT)^2 r^6}\left\{\frac{3\tau_{c3}}{(1+\omega_I{}^2\tau_{c3}{}^2)}\right\} + R_{\text{contact}}$$

$$(\tau_{c1})^{-1} = (\tau_{e1})^{-1} + (\tau_r)^{-1} + (\tau_M)^{-1}$$

$$(\tau_{c2})^{-1} = (\tau_{e2})^{-1} + (\tau_r)^{-1} + (\tau_M)^{-1}$$

$$(\tau_{c3})^{-1} = (\tau_M)^{-1} + (\tau_r)^{-1} \qquad (2)$$

where μ_o is the magnetic permeability of vacuum, μ_B is the electron Bohr magneton, J is the total angular momentum quantum number of the paramagnetic species, g_J is the corresponding g factor, γ_I is the proton magnetogyric ratio, ω_I and ω_S are the proton and the electron precession frequencies, τ_r is the rotational correlation time of CsA, τ_M the lifetime of the metal−peptide complex, τ_e is the electronic relaxation time of the metal ion (1 and 2 indicate longitudinal and transversal components), and r is the metal−proton distance. The equation accounts for the spin−orbit coupling, which is not negligible when dealing with lanthanides.[38,39] From the above relation, it is clear that, if one metal−proton distance and the correlation time are known, R_1^{para} can be estimated (contact contribution arising from direct electron-spin density on the nucleus can be neglected in some cases, vide infra). This value can be used with the experimental relaxation rate in eq 1 to obtain the molar fractions p^{free} and p^{bound} and consequently all other metal−proton distances from the other experimental rates.

The analysis of longitudinal relaxation rate enhancements, ΔR_1, shows conspicuous changes for ^{7}Ala-Hα and ^{8}D-Ala-Hα (Figure 5). Large effects are also detected for ^{8}D-Ala-Hβ and ^{9}MeLeu-NMe, indicating a metal coordination at the carbonyl oxygen of ^{8}D-Ala, in agreement with the strong preference of calcium and lanthanides toward oxygen donors. Imposing a direct bond between the metal and the oxygen, the Dy(III)-^{8}D-Ala-Hα distance is found within the range 0.25−0.40 nm. In fact, the small contribution to ^{9}MeLeu *N*-methyl selects only one of the two possible orientations of the metal with respect to the carbonyl oxygen in trigonal planar geometry. As for the evaluation of the correlation time, R_{Solomon} is mainly modulated by the electron spin relaxation time in the range 0.1−1 ps.[39] In fact, (i) the exchange time, τ_M, is quite longer than 1 ps and

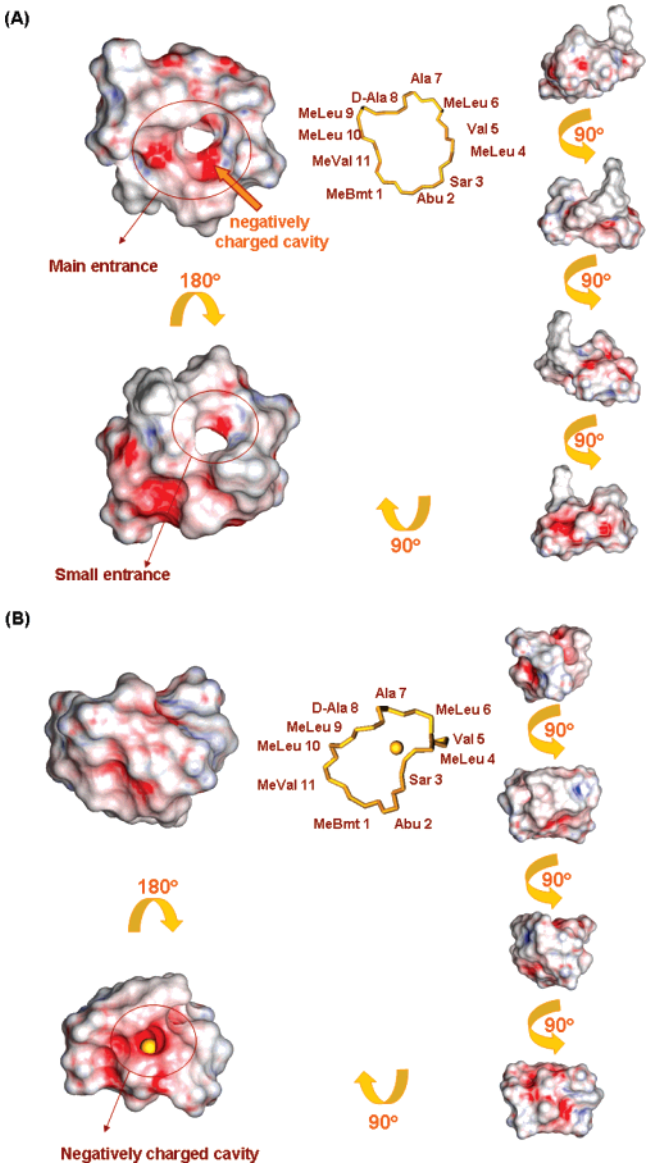

Figure 3. Electrostatic potential surface of (A) free CsA in SDS environment and (B) CsA-Dy(III) complex; positively and negatively charged regions are shown in blue and red, respectively. For each structure, two larger views are shown, rotated by 180° with respect to one another. For the first view of the potential surface of each structure, the backbone orientation is reported.

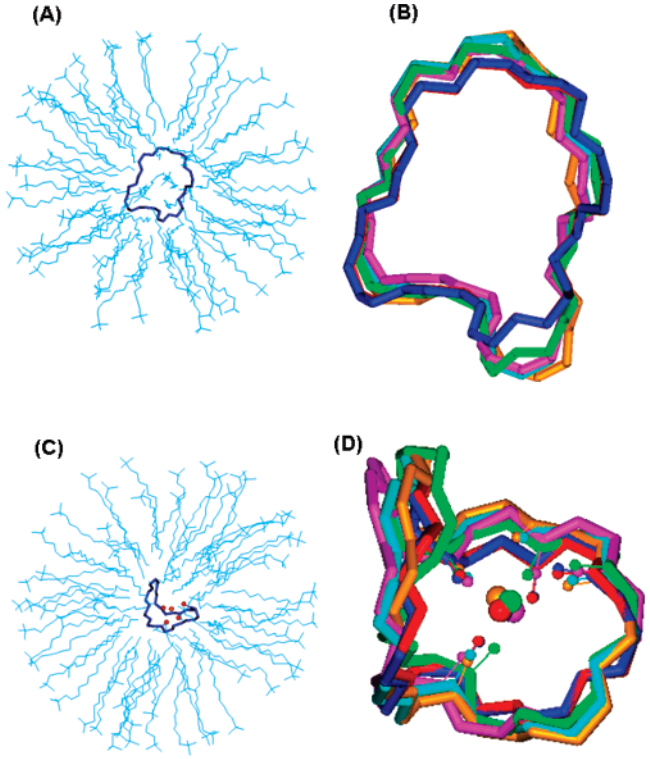

Figure 4. Best experimental structure of free CsA positioned inside the micelle core (A); comparison of free CsA conformation obtained from experimental data with those at various stages of the MD simulation in H_2O/SDS environment (B); best experimental structure of CsA−Dy(III) complex positioned inside the micelle core (C); comparison of complex conformation obtained from experimental data with those at various stages of the MD simulation in H_2O/SDS (D). Color codes in B and D are the following: best structure resulting from DYANA program (blue), after energy minimization (red), brought to 298 K (green), snapshots taken during the MD simulation (magenta, cyan, and dark orange).

cannot affect the value of R_1^{para} in eq 2. τ_M could in principle obscure the paramagnetic contributions to the measured relaxation rates when it is in the same order of magnitude of R_1^{bound} or larger; under these circumstances, similar relaxation enhancements should be found everywhere in the molecule, which was not the case; (ii) a rotational correlation time, τ_r, of 6.8 ns was calculated from the Stokes equation considering the micelle constituted of 60 SDS molecules as reported elsewhere.[40] The same τ_r value was used to evaluate R_{Curie} in eq 2.

Once one reference distance of Dy(III)-^{8}D-Ala-Hα is set, the molar fraction p^{bound} of CsA can be estimated from eqs 1 and 2 and can be used to back-calculate all other distances. These were almost independent of τ_e (ranging between 0.1 and 1 ps), since the dependence of both p^{bound} and R^{bound} on τ_e practically cancels out in the combination of eqs 1 and 2.

Contact contribution in eq 2 was neglected. Four sets of distances were obtained corresponding to values of Dy(III)-^{8}D-Ala-Hα distance of 0.25, 0.30, 0.35, and 0.40 nm. Out of these, only the last gave good results in terms of distance violations (Table 2, Figure 2B). Target function values (proportional to the sum of squared distance violations) were in fact in the order of 30, 20, 8, and 1 respectively for each run. The chosen reference distance is compatible with small p^{bound} values between 4.2×10^{-4} and 1.17×10^{-3} (uncertainty is related to the uncertainty in the electronic relaxation times), because of the fact that Dy(III) also interacts with the much more abundant SDS (vide infra). The value of rmsd (for the best five structures backbone rmsd is 0.12 nm; 0.16 nm for the first 30) found for the CsA−Dy(III) complex structure indicates that the definition is not as high as for the solution structure of the free ligand.

On the best experimental structure, an energy minimization and a molecular dynamics simulation in H_2O/SDS were performed with the CsA molecule placed in the core of the micelle (Figure 4C,D).

The coordination of dysprosium ion may involve, besides ^{8}D-Ala, carbonyl oxygens of residues ^{3}Sar, ^{4}MeLeu, and ^{5}Val, as also indicated by the observed approaching of these atoms to the dysprosium ion during the MD trajectory.

Stoichiometry and Stability of the Complex. Given the high SDS to CsA ratio, we can assume that only one CsA molecule lies within each micelle, excluding the formation of $(CsA)_n$−Dy(III) complexes. The insertion of the metal within the CsA cavity also supports this picture.

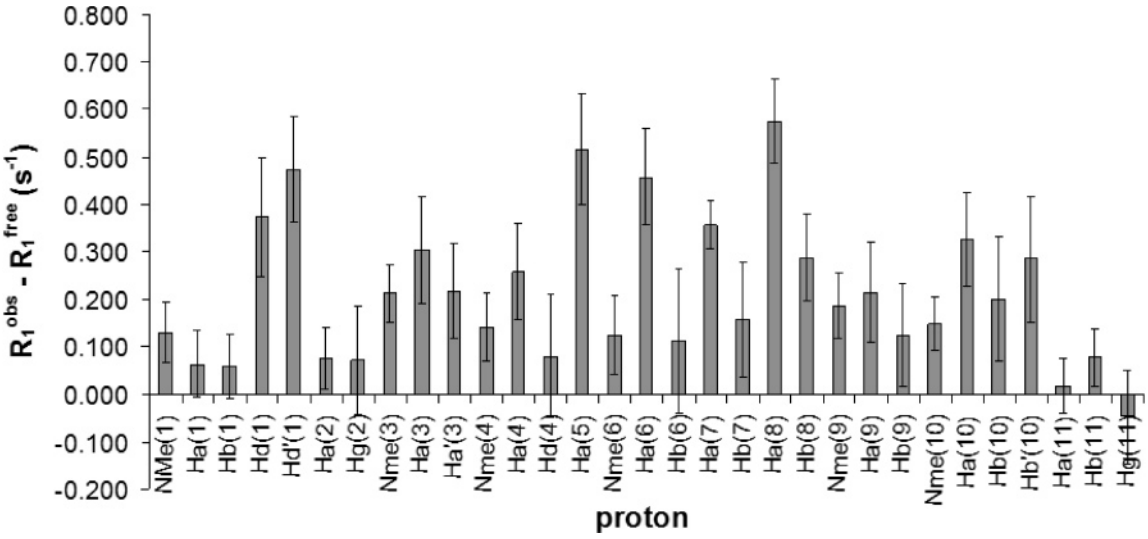

Figure 5. Relaxation rate variations, $R_1^{obs} - R_1^{free}$ (s^{-1}) of the CsA−Dy(III) complex in micelles at 298 K with respect to the free form, with error bars corresponding to the estimated error.

TABLE 2: Metal-Proton Distances (Upper and Lower Limits) for the CsA−Dy(III) Complex, Obtained from Paramagnetic Relaxation Contributions through the Solomon−Curie Equation

residue	atom	*r*_lower (nm)	*r*_upper (nm)
[1]MeBmt	HN	0.48	0.57
[1]MeBmt	Hα	0.51	
[1]MeBmt	Hβ	0.51	
[1]MeBmt	Hδ	0.41	0.46
[1]MeBmt	Hδ'	0.4	0.43
[2]Abu	Hα	0.505	0.77
[2]Abu	Hγ	0.48	
[3]Sar	HN	0.45	0.5
[3]Sar	Hα	0.42	0.48
[3]Sar	Hα′	0.44	0.52
[4]MeLeu	HN	0.47	0.57
[4]MeLeu	Hα	0.43	0.5
[4]MeLeu	Hδ	0.47	
[5]Val	Hα	0.39	0.425
[6]MeLeu	HN	0.47	0.61
[6]MeLeu	Hα	0.4	0.43
[6]MeLeu	H	0.45	
[7]Ala	Hα	0.42	0.44
[7]Ala	Hβ	0.45	0.63
[8]D−Ala	Hα	0.39	0.41
[8]D−Ala	Hβ	0.43	0.48
[9]MeLeu	HN	0.46	0.52
[9]MeLeu	Hα	0.44	0.53
[9]MeLeu	Hβ	0.465	0.71
[10]MeLeu	HN	0.475	0.54
[10]MeLeu	Hα	0.42	0.47
[10]MeLeu	Hβ	0.44	0.565
[10]MeLeu	Hβ'	0.42	0.5
[11]MeVal	Hα	0.56	
[11]MeVal	Hβ	0.51	0.72

Knowledge of the molar fractions of bound and free CsA allowed the estimation of the dissociation constant. It is important to point out that Dy(III) does interact with SDS molecules in consequence of its affinity for sulfate groups, similarly to Ca(II) ion.

Concentrations at the equilibrium were in fact calculated as follows:

$$[\mathrm{CsADy}] = p^{\mathrm{bound}} C_{\mathrm{CsA}}$$

$$[\mathrm{CsA}] = p^{\mathrm{free}} C_{\mathrm{CsA}}$$

$$[\mathrm{Dy}] = C_{\mathrm{Dy}} - [\mathrm{CsADy}] - [(\mathrm{SDS})_n\mathrm{Dy}] = C_{\mathrm{Dy}} - p^{\mathrm{bound}} C_{\mathrm{CsA}} - p^{\mathrm{SDS}} C_{\mathrm{Dy}}$$

$$K_{\mathrm{d}} = \frac{[\mathrm{CsA}][\mathrm{Dy}]}{[\mathrm{CsADy}]} \tag{3}$$

where C indicates the analytical concentration, K_{d} is the dissociation constant, and p^{SDS} is the molar fraction of Dy(III) bound to SDS.

In order to evaluate the molar fraction of SDS bound to Dy(III) ion, we calculated the dissociation constant of the Dy(III)−(SDS) complex (K_{d} = 99.3 mM) plotting Dy(III) ion concentration as a function of the chemical shift variation of SDS signals and fitting them with a nonlinear function:

$$C_{\mathrm{Dy}} = \frac{C_{\mathrm{SDS}}\Delta^2 - K_{\mathrm{d}}\Delta_0\Delta - C_{\mathrm{SDS}}\Delta_0\Delta}{\Delta_0\Delta - \Delta_0^{\,2}} \tag{4}$$

This equation results from the following relation:[41]

$$\Delta = \Delta_0 \frac{C_{\mathrm{Dy}}^{\mathrm{free}}}{K_{\mathrm{d}} + C_{\mathrm{Dy}}^{\mathrm{free}}} \tag{5}$$

where Δ is the actual change of chemical shift, Δ_0 is the limit value of the chemical shift variation, $C_{\mathrm{Dy}}{}^{\mathrm{free}}$ is the experimental dysprosium concentration corrected by using the relation:

$$C_{\mathrm{Dy}}^{\mathrm{free}} = C_{\mathrm{Dy}} - C_{\mathrm{SDS}} \frac{\Delta}{\Delta_0} \tag{6}$$

where C_{Dy} and C_{SDS} are the analytical concentration of Dy(III) and SDS. respectively.

Given the analytical concentration of SDS and Dy(III) and p^{SDS}, we found a value for K_{d} of 160 mM for the CsA−Dy(III) which indicates the formation of a weak complex in agreement with the fast exchange conditions detected.

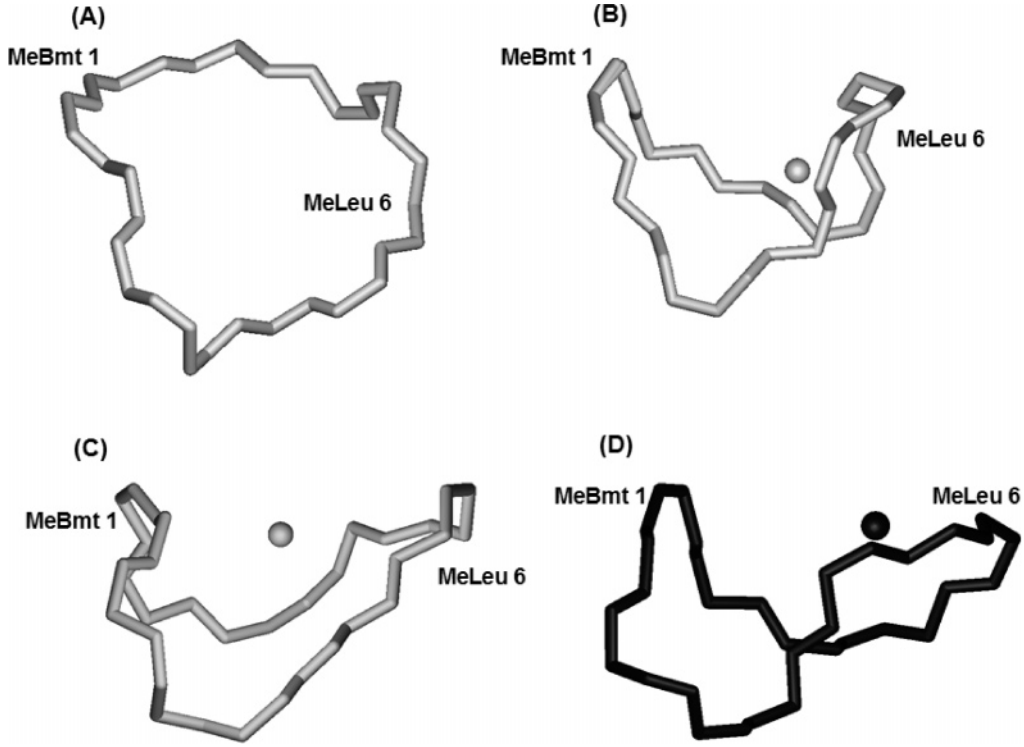

Figure 6. Comparison between the backbone structure of free CsA in H_2O/SDS (A), CsA−Dy(III) complex in H_2O/SDS (B), CsA−Ce(III) complex in acetonitrile (C), and CsA−Mg(II) complex in acetonitrile (D).

Discussion

The solution structures of cyclosporin A free and bound to calcium-mimicking dysprosium ion allow us to understand the conformational changes brought about by the metal ion. Defining the solution structure of weak complexes is not an easy task because of the small effects induced on the ligands by the metal ion. The use of strongly paramagnetic probes is of substantial help in this cases as shown by the present work. The low value of the rmsd of the free form is probably due to the structuring effect of micelles which really select one single conformation out of the many possible in water (Figure 1).

The comparison of electrostatic potential surfaces of CsA free and bound to the metal ion suggests the mechanism of formation of the complex and explains the structural modifications induced by Dy(III). In the surface of the free ligand, the presence of a negatively charged channel that may host positively charged metal ions (Figure 3A) is apparent. A closer inspection of the electrostatic potential reveals that the carbonyl oxygen of ^{3}Sar yields the main contribution to the charge in the cavity, being the carbonyl oxygen of ^{11}MeVal also important as an anchoring point at the entrance of the tunnel (Figure 3A). The central part of the cavity where ^{3}Sar carbonyl oxygen resides can host a 0.24 nm radius sphere. Entrance from the opposite site of the channel seems less favorable since the channel is narrower. The available room for the main entrance is approximately a 0.3 nm radius sphere, while the opposite side has a radius of about 0.16 nm.

Although the ionic radius of Dy(III) (and also Ca(II)) is about 0.1 nm, the hydration sphere makes it at least 0.14 nm larger reaching a final value of at least 0.24 nm. Entrance of the metal ion from the smaller site would be possible only if the coordinating atoms were well-exposed to the solvent allowing a direct replacement of water molecules from the coordination sphere. The solvated metal ion can instead enter the main cavity attracted by the carbonyl oxygen of ^{11}MeVal and can even reach the central part of the cavity to replace the water ligands for the carbonyl donors of CsA. In order to accommodate the new coordinating atoms, the circular backbone structure, which is well-opened (Figure 6), has to be compressed to reduce the internal cavity from 0.24 nm to about 0.1 nm (the ionic radius of the metal); this results in a rearrangement of the CsA molecule which implies the formation of a calyx containing the metal in a 0.15 nm radius spherical space. As shown in Figure 3B, the electrostatic potential of this new metal site is highly negatively charged because of the exposition, inside the cavity, of the previously buried coordinating carbonyl donors of CsA. The coordination of dysprosium ion involves carbonyl oxygens of residues ^{3}Sar, ^{4}MeLeu, ^{5}Val, and ^{8}D-Ala. Since dysprosium is known to adopt a coordination geometry with six or eight ligands, the involvement of oxygens of water molecules to complete the coordination sphere can be hypothesized. The structure obtained from experimental data shows that there is enough room in the cavity of CsA molecule to accommodate up to two water molecules coming from the solvated metal ion. Moreover the average structure during the MD simulation also maintains an internal cavity that can host two molecules of water (Figure 7A,B).

A comparison of the CsA−Dy(III) complex with existing experimental structures of CsA bound to Cyp would help in understanding the role of the metal in the interaction. However, one must consider that the two structures were solved in different conditions. While the bound structures of CsA were solved in water, our complex is in micelles. The micellar environment, which vehicles the drug to the cell membrane, is likely to affect the conformation of CsA. Indeed, the Cyp-bound form of CsA, being essentially planar, is very different from other metal bound structures.[17] The role of the metal, if present, would be to expose only one part of the molecule in the proper conformation for the interaction with Cyp. Unfortunately, the low resolution of our complex makes a detailed local comparison with the Cyp-bound form difficult. Regarding the comparison with the other metal complexes, instead,[17] the overall shape resembles that of

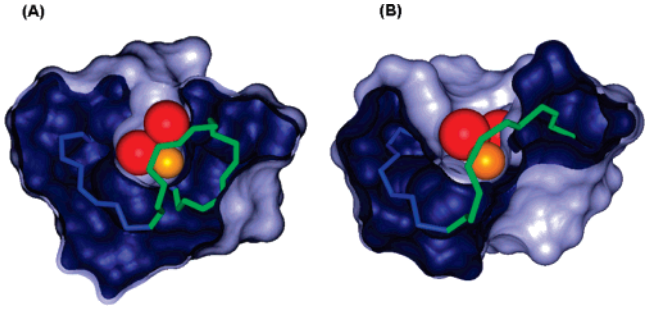

Figure 7. van der Waals surface of the CsA−Dy(III) complex, showing that in the cavity of CsA there is enough room to accommodate up to two water molecules coming from the solvated metal ion. (A) Best experimental structure, (B) average structure during the MD simulation. The water molecules are shown as red spheres, and the Dy(III) ion is shown as a gold sphere.

the Ce(III) complex in CH_3CN, being CsA folded around the metal in both cases, in agreement with the similar coordination properties of these two metals, both used as Calcium mimics.

Acknowledgment. This work was supported by the MIUR FIRB RBNE03PX83_003. We acknowledge C.I.R.M.M.P. (Consorzio Interuniversitario Risonanze Magnetiche di Metalloproteine Paramagnetiche) for financial support.

Supporting Information Available: List of the NOE-derived distance restraints used for structure determination of free CsA in H_2O/SDS, plots of the chemical shift variations as a function of temperature for the mobile protons of free CsA in micelles. This material is available free of charge via the Internet at http://pubs.acs.org.

References and Notes

(1) Wenger, R. M. *Angew. Chem.* **1985**, *24*, 77−85.
(2) Neri, P.; Meadows, R.; Gemmecker, G.; Olejniczak, E.; Nettesheim, D.; Logan, T.; Simmer, R.; Helfrich, R.; Holzman, T.; Severin, J.; Fesik, S. *FEBS Lett.* **1991**, *294*, 81−88.
(3) Schreiber, S. L.; Albers, M. W.; Brown, E. J. *Acc. Chem. Res.* **1993**, *26*, 412−420.
(4) Klee, C. B.; Ren, H.; Wang, X. *J. Biol. Chem.* **1998**, *273*, 13367−13370.
(5) Hsu, W.; Heald, S. L.; Harding, M. W.; Handschumacher, R. E.; Armitage, I. M. *Biochem. Pharmacol.* **1990**, *40*, 131−140.
(6) Loosli, H.-R.; Kessler, H.; Oschkinat, H.; Weber, H.-P.; Petcher, T. J.; Widmer, A. *Helv. Chim. Acta* **1985**, *68*, 682−703.
(7) Kessler, H.; Loosli, H.-R.; Oschkinat, H. *Helv. Chim. Acta* **1985**, *68*, 661−681.
(8) Klages, J.; Neubauer, C.; Coles, M.; Kessler, H.; Luy, B. *Chem. Biol. Chem.* **2005**, *6*, 1672−1678.
(9) Ran, Y.; Zhao, L.; Xu, Q.; Yalkowsky, S. H. *AAPS Pharm. Sci. Tech.* **2001**, *2*, E2.
(10) El Tayar, N.; Mark, A. E.; Vallat, P.; Brunne, R. M.; Testa, B.; van Gunsteren, W. F. *J. Med. Chem.* **1993**, *36*, 3757−3764.
(11) Potter, B.; Palmer, R. A.; Withnall, R.; Jenkins, T. C.; Chowdhry, B. Z. *Org. Biomol. Chem.* **2003**, *1*, 1466−1474.
(12) Weber, C.; Wider, G.; von Freyberg, B.; Traber, R.; Braun, W.; Widmer, H.; Wuthrich, K. *Biochemistry* **1991**, *30*, 6563−6574.
(13) Fesik, S. W.; Gampe, R. T.; Holzman, T. F.; Egan, D. A.; Edalji, R.; Luly, J. R.; Simmer, R.; Helfrich, R.; Kishore, V.; Rich, D. H. *Science* **1990**, *250*, 1406−1409.
(14) Theriault, Y.; Logan, T. M.; Meadows, R.; Yu, L.; Olejniczak, E. T.; Holzman, T. F.; Simmer, R. L.; Fesik, S. W. *Nature* **1993**, *361*, 88−91.
(15) Wüthrich, K.; von Freyberg, B.; Weber, C.; Wider, G.; Traber, R.; Widmer, H.; Braun, W. *Science* **1991**, *254*, 953−954.
(16) Kock, M.; Kessler, H.; Seebach, D.; Thaler, A. *J. Am. Chem. Soc.* **1992**, *114*, 2676−2686.
(17) Bernardi, F.; Gaggelli, E.; Molteni, E.; Porciatti, E.; Valensin, D.; Valensin, G. *Biophys. J.* **2006**, *90*, 1350−1360.
(18) Kahan, B. D. *N. Engl. J. Med.* **1989**, *321*, 1725−1738.
(19) Matsuda, S.; Koyasu, S. *Immunopharmacology* **2000**, *47*, 119−125.
(20) Dancer, R. J.; Jones, A.; Fairlie, D. P. *Aust. J. Chem.* **1995**, *48*, 1835−1841.
(21) Carver, J. A.; Rees, N. H.; Turner, D. L.; Senior, S. J.; Chowdhry, B. Z. *J. Chem. Soc., Chem. Commun.* **1992**, *22*, 1682−1684.
(22) Cusack, R.; Grondhal, L.; Fairlie, D.; Hanson, G.; Gahan, L. *J. Inorg. Biochem.* **2003**, *97*, 191−198.
(23) Lee, E. J.; Lee, S. W.; Choi, H. G.; Kim, C. K. *Int. J. Pharm.* **2001**, *218*, 125−131.
(24) Francis, M. F.; Lavoie, L.; Winnik, F. M.; Leroux, J. C. *Eur. J. Pharm. Biopharm.* **2003**, *56*, 337−346.
(25) Rangel-Yagui, C. O.; Pessoa, A., Jr.; Costa Tavares, L. *J. Pharm. Pharmaceut. Sci.* **2005**, *8*, 147−163.
(26) Harris, R. K.; Becker, E. D.; Cabral de Menezes, S. M.; Goodfellow, R.; Granger, P. *Pure Appl. Chem.* **2001**, *73*, 1795−1818.
(27) Hwang, T. L.; Shaka, A. J. *J. Magn. Reson. A* **1995**, *112*, 275−279.
(28) Mumenthaler, C.; Güntert, P.; Braun, W.; Wüthrich, K. *J. Biomol. NMR* **1997**, *10*, 351−362.
(29) Güntert, P;, Mumenthaler, C.; Wüthrich, K. *J. Mol. Biol.* **1997**, *273*, 283−298.
(30) Lindahl, E.; Hess, B.; van der Spoel, D. *J. Mol. Model.* **2001**, *7*, 306−317.
(31) Berendsen, H.; van der Spoel, D.; van Drunen, R. *Comput. Phys. Commun.* **1995**, *91*, 43−56.
(32) van Gunsteren, W. F.; Daura, X.; Mark, A. *Encyclopaedia of Computational Chemistry* **1998**, *2*, 1211−1216.
(33) Berendsen, H.; Postma, J.; van Gunsteren, W. F.; Di Nola, A.; Haak, J. *J. Chem. Phys.* **1984**, *81*, 3684−3690.
(34) Ryckaert, J.; Ciccotti, G.; Berendsen, H. *J. Comput. Phys.* **1977**, *23*, 327−341.
(35) Berendsen, H. In *Molecular Dynamics and Protein Structure;* Hermans, J., Ed.; Polycrystal Book Service: Western Springs, U.S.A., 1995; pp 18−22.
(36) Brito, R. M.; Vaz, W. L. *Anal. Biochem.* **1986**, *152*, 250−255.
(37) Baxter, N. J.; Williamson, M. P. *J. Biomol. NMR* **1997**, *9*, 359−369.
(38) Solomon, I. *Phys. Rev.* **1955**, *99*, 559−565.
(39) Bertini, I.; Luchinat, C. *Coord. Chem. Rev.* **1996**, *150*, 1−294.
(40) Budavari, S. *The Merck Index: An Encyclopedia of Chemicals, Drugs and Biologicals*, 12th ed.; Whitehouse Station: New Jersey, 1996; p 8782.
(41) D'Amelio, N.; Gaggelli, E.; Gaggelli, N.; Mancini, F.; Molteni, E.; Valensin, D.; Valensin, G. *J. Inorg. Biochem.* **2003**, *95*, 225−229.